

See discussions, stats, and author profiles for this publication at: <https://www.researchgate.net/publication/274643943>

# EDB Fibronectin Specific Peptide for Prostate Cancer Targeting

ARTICLE *in* BIOCONJUGATE CHEMISTRY · APRIL 2015

Impact Factor: 4.51 · DOI: 10.1021/acs.bioconjchem.5b00178 · Source: PubMed

---

CITATIONS

2

---

READS

46

## 10 AUTHORS, INCLUDING:



Zheng Han

Case Western Reserve University

2 PUBLICATIONS 3 CITATIONS

[SEE PROFILE](#)



Zhuxian Zhou

Zhejiang University

32 PUBLICATIONS 431 CITATIONS

[SEE PROFILE](#)



Cristina Magi-Galluzzi

Cleveland Clinic

190 PUBLICATIONS 5,136 CITATIONS

[SEE PROFILE](#)



Zheng-Rong Lu

Case Western Reserve University

123 PUBLICATIONS 3,389 CITATIONS

[SEE PROFILE](#)

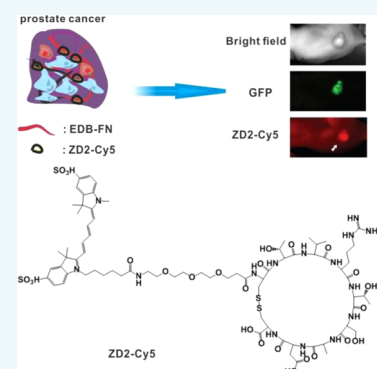
## EDB Fibronectin Specific Peptide for Prostate Cancer Targeting

Zheng Han,<sup>†</sup> Zhuxian Zhou,<sup>†</sup> Xiaoyue Shi,<sup>†</sup> Junpeng Wang,<sup>†</sup> Xiaohui Wu,<sup>†</sup> Da Sun,<sup>†</sup> Yinghua Chen,<sup>‡</sup> Hui Zhu,<sup>§</sup> Cristina Magi-Galluzzi,<sup>||</sup> and Zheng-Rong Lu<sup>\*,†</sup>

<sup>†</sup>Department of Biomedical Engineering and <sup>‡</sup>Department of Physiology and Biophysics, Case Western Reserve University, Cleveland, Ohio 44106, United States

<sup>§</sup>Glickman Urological Institute, and <sup>||</sup>Robert J. Tomsich Pathology and Laboratory Medicine Institute, Cleveland Clinic Foundation, Cleveland, Ohio 44106, United States

**ABSTRACT:** Extradomain-B fibronectin (EDB-FN), one of the oncofetal fibronectin (onfFN) isoforms, is a high-molecular-weight glycoprotein that mediates cell adhesion and migration. The expression of EDB-FN is associated with a number of cancer-related biological processes such as tumorigenesis, angiogenesis, and epithelial-to-mesenchymal transition (EMT). Here, we report the development of a small peptide specific to EDB-FN for targeting prostate cancer. A cyclic nonapeptide, CTVRTSADC (ZD2), was identified using peptide phage display. A ZD2-Cy5 conjugate was synthesized to accomplish molecular imaging of prostate cancer *in vitro* and *in vivo*. ZD2-Cy5 demonstrated effective binding to up-regulated EDB-FN secreted by TGF- $\beta$ -induced PC3 cancer cells following EMT. Following intravenous injections, the targeted fluorescent probe specifically bound to and delineated PC3-GFP prostate tumors in nude mice bearing the tumor xenografts. ZD2-Cy5 also showed stronger binding to human prostate tumor specimens with a higher Gleason score (GS9) compared to those with a lower score (GS 7), with no binding in benign prostatic hyperplasia (BPH). Thus, the ZD2 peptide is a promising strategy for molecular imaging and targeted therapy of prostate cancer.



### INTRODUCTION

Prostate cancer (PCa) is the second most lethal form of cancer affecting men in the United States.<sup>1</sup> The lifetime risk of being diagnosed with PCa is about 1 in 7, making PCa a potential epidemic health problem in men. Early detection and timely treatment is critical to improve the survival of patients diagnosed with high-risk PCa. Prostate-specific antigen (PSA) screening is routinely used in detecting PCa, and has resulted in a significant decrease in PCa mortality due to early treatment.<sup>2</sup> However, PSA screening for PCa detection remains controversial, because nonmalignant conditions such as benign prostatic hyperplasia (BPH) can also present with elevated PSA levels.<sup>2,3</sup> In fact, a significant proportion of PCa diagnosed through PSA screening are considered to be low risk and indolent. Even so, most patients with low risk PCa are prescribed treatment to avoid potential undertreatment, leading to treatment-related long-term side effects. Out of concern that the risks of overtreatment may outweigh the benefits of PSA screening, the US Preventive Services Task Force recommended against PSA screening in 2012, despite the significant decrease in PCa mortality rate since the introduction of PSA screening in the early 1990s.<sup>4,5</sup> Consequently, there is an urgent demand for highly accurate diagnostic tools for the noninvasive detection of high-risk PCa.

Malignant tumors have a unique microenvironment, which facilitates cancer cell survival, proliferation, and metastasis. The extracellular matrix (ECM) of malignant tumors exhibits an abnormally high expression of cancer-related proteins. For example, oncofetal fibronectin (onfFN), one of the most

abundant ECM components,<sup>6</sup> plays a key role in tumorigenesis,<sup>7,8</sup> angiogenesis,<sup>9,10</sup> and metastasis.<sup>11,12</sup> Various human cancers,<sup>13–15</sup> including PCa,<sup>4,16–19</sup> demonstrate the presence of onfFN. In addition, increased expression of onfFN isoforms, including extradomain-B fibronectin (EDB-FN), is inversely correlated with patient survival.<sup>13,20,21</sup> OnfFN mediates cell migration and invasion, both of which are essential for the stroma–cancer interaction during the development of PCa.<sup>15</sup> EDB-FN is a known marker of angiogenesis and epithelial–mesenchymal transition (EMT),<sup>17</sup> a process that initiates cancer metastasis<sup>11</sup> and generates invasive mesenchymal cells in high-grade prostate tumors.<sup>22,23</sup> Thus, the elevated expression of EDB-FN is a promising biomarker for the detection and diagnosis of high-risk PCa. By virtue of its abundance in the tumor ECM and its accessibility to molecular probes and imaging agents, EDB-FN is also a suitable molecular target for molecular imaging, imaging-guided surgery, and tumor-specific drug delivery.

We set out to develop small peptide sequences that can specifically bind to EDB-FN for PCa targeting and imaging. Although EDB-FN-specific antibodies have been developed in the past, small peptides are advantageous, due to their lack of immunogenicity, cost-efficient production, and relatively simple development for translational studies. In this report, we used phage display to identify a small peptide specific to EDB-FN. A fluorescent imaging probe of the peptide was synthesized for

Received: January 23, 2015

Published: April 7, 2015

imaging the protein marker EDB-FN in PCa. The binding property of the peptide to EDB-FN was investigated *in vitro* and *in vivo*. In addition, the PCa targeting potential of the peptide was investigated in a mouse prostate tumor model and human PCa specimens of different grades.

## RESULTS

**EDB-FN Binding Peptide.** The EDB fragment is a type-III-homology repeat with a highly conserved sequence of 91 amino acids encoded by a single exon.<sup>13</sup> The plasmid construction scheme is shown in Figure 1A. EDB-FN was successfully

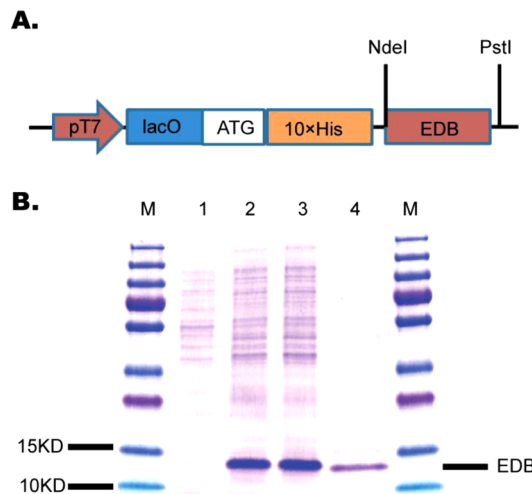


**Figure 1.** Construction of the EDB-expressing plasmid and SDS-PAGE assay of lysates from EDB-expressing *E. coli* strain BL21. (A) The DNA-encoding EDB fragment was inserted under the control of T7 promoter, along with 10 His tags at the N-terminal. The Lac operator (lacO) allows for the control of EDB expression with IPTG induction. (B) Stained gel with the lanes labeled as follows: M, protein ladder; 1, BL21 cell lysate before induction with IPTG; 2, 1.5 h post-induction; 3, 3 h post-induction; and 4, purified EDB solution from lysate acquired 3 h after induction.

expressed in *E. coli* and SDS-PAGE was performed to confirm the size and purity of the EDB fragment (Figure 1B). Four rounds of panning yielded an enriched phage library containing phages with high EDB binding ability. Out of the 29 selected phage clones, the peptide sequence CTVRTSADC appeared 5 times. This peptide was named ZD2 and identified as the lead peptide for targeting EDB-FN.

Cyclic ZD2 peptide (CTVRTSADC) was synthesized using standard solid-phase peptide chemistry. The peptide was then labeled with the fluorescent chromophore cyanine 5 (Cy5) through a short PEG linker to obtain the fluorescent peptide probe ZD2-Cy5 (Figure 2A). The MALDI-TOF mass spectrum of ZD2-Cy5 is shown in Figure 2B. Surface plasmon resonance (SPR) was used to characterize the interaction between the cyclic ZD2 peptide and EDB protein. EDB was immobilized onto the chip surface, through the reaction of carboxyl groups on the chip with the amine group on EDB. Since EDB contains only one amine group at the N-terminus, this immobilization method results in a uniform steric orientation of EDB, thereby optimizing site exposure for ZD2 binding. Sensorgrams were generated by flowing ZD2 peptide solutions of 1.9  $\mu$ M to 250  $\mu$ M over the chip surface (Figure 3A). A Scatchard plot of saturation levels at different concentrations indicates that the binding response was not a simple Langmuir equilibrium

binding isotherm (Figure 3B).<sup>24</sup> Two binding sites were identified by fitting data from 1.9  $\mu$ M to 7.8  $\mu$ M or data from 15.6  $\mu$ M to 250  $\mu$ M. A tight binding site had an affinity of 11  $\mu$ M, and a weak site was measured to have an affinity of 384  $\mu$ M. Considering the short length of ZD2, the binding to the tight binding site is biologically competent for *in vivo* targeting studies.

**In Vitro Binding of ZD2-Cy5 to EDB-FN Secreted by TGF- $\beta$ -Induced PC3 Prostate Cancer Cells.** Elevated expression of onfFN is a marker of EMT in PCa cells. The treatment of PC3-GFP human PCa cells with TGF- $\beta$  resulted in an elongated mesenchymal phenotype, as compared with cells without TGF- $\beta$  treatment (Figure 4A). Up-regulation of the mRNA expression level of EDB-FN was confirmed by quantitative RT-PCR ( $p < 0.05$ ) (Figure 4B). TGF- $\beta$  induction leads to the binding of ZD2-Cy5 in the medium (0.25  $\mu$ M) to the fibrillary network of EDB-FN secreted by the induced cells. As shown in Figure 4C, GFP signal delineates the boundary of the PC3 cells, while red fluorescence clearly reveals high accumulation of ZD2-Cy5 at the cell periphery. Preincubation of the induced cells with medium containing 25  $\mu$ M free ZD2 peptide blocked the binding of ZD2-Cy5 due to competitive binding. ZD2-Cy5 did not exhibit significant binding to noninduced PC3 cells. In addition, the control probe CERAK-Cy5 (25  $\mu$ M) showed negligible binding to induced PC3 cells (Figure 4C). Further quantitative analysis of the Cy5 fluorescence intensity of peptide binding was also performed to validate the enhanced binding of ZD2-Cy5 to the TGF- $\beta$ -induced PC3 cells (Figure 4D). These results demonstrate that ZD2-Cy5 specifically binds to EDB-FN secreted by TGF- $\beta$ -induced PC3 cells.

**In Vivo Binding of ZD2-Based Imaging Probes in Mouse PC3 Prostate Tumor Model.** The *in vivo* targeting of ZD2 to prostate tumors was demonstrated by fluorescence imaging of mice bearing PC3-GFP flank tumor xenografts after intravenous injection of ZD2-Cy5 (Figure 5). At 1.5 h after injection, ZD2-Cy5 exhibited strong binding to the GFP-labeled prostate tumor, while no apparent accumulation was seen for the control CERAK-Cy5 in the tumor. At 3 h after injection, the overall Cy5 signal in mice decreased due to systemic clearance of the peptide probe, but the tumor-to-normal signal ratio (T/N ratio) remained unchanged for ZD2-Cy5. At the 3 h time point, the T/N ratio of ZD2-Cy5 was around 2, while that of CERAK-Cy5 was around 1 (Figure 5B). The mice were sacrificed 5 h after injection, and the tumor and major organs were collected and imaged to further verify the *in vivo* targeting specificity of Cy5-labeled ZD2 in the tumors. As shown in Figure 5C, ZD2-Cy5 shows significant signal in the tumor, and comparatively lower signal in the normal organs and tissues, confirming specific *in vivo* targeting of the peptide to prostate tumor. The control CERAK-Cy5 showed little accumulation in both tumor and normal organs. In addition, an *in vivo* competitive study was performed by coinjecting a mixture of 1  $\mu$ M cyclic ZD2 and 10 nmol ZD2-Cy5, which resulted in decreased signal in the tumor, indicating that the binding between ZD2 and the tumor is mediated through a specific site, i.e., EDB-FN. Western blot analysis of protein lysates from the organs showed that PC3 tumor expresses substantially more EDB-FN than the liver and lung (Figure 5D). Histological analysis of the tissue sections from the tumor-bearing mice injected with ZD2-Cy5 showed that the Cy5 signal is in the ECM of the tumor, which further confirms the tumor-specificity of ZD2-Cy5 (Figure 6A). No accumulation of

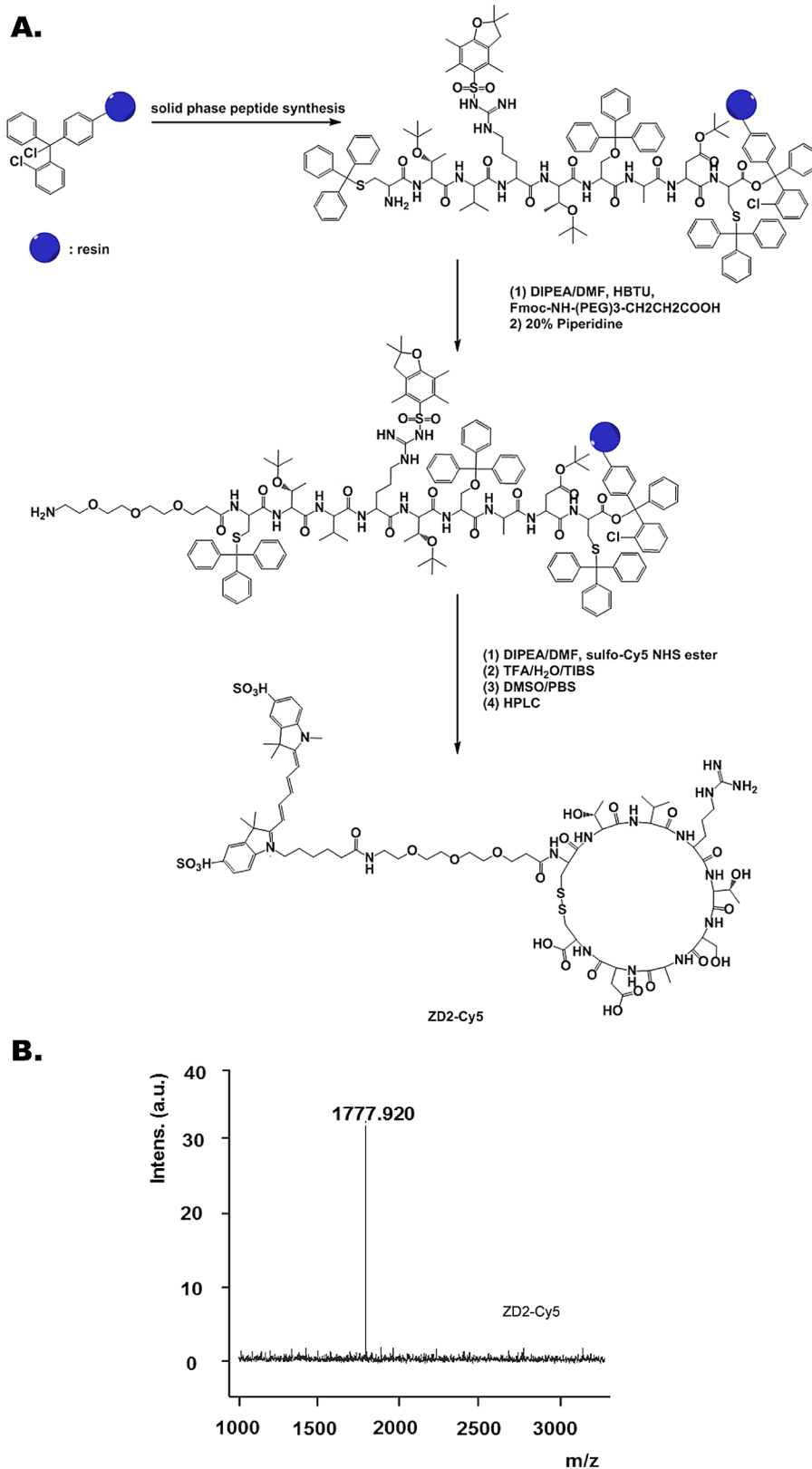


**Figure 2.** Schematic illustration of the (A) synthesis of ZD2-Cy5 and (B) MALDI-TOF mass spectrum of ZD2-Cy5.

ZD2-Cy5 was found in the liver or lung sections (Figure 6B). EDB-FN is a known biomarker of tumor angiogenesis and its expression is associated with angiogenesis.<sup>13</sup> The binding of ZD2-Cy5 in the prostate tumor sections was further correlated with immunofluorescence staining of EDB-FN and CD31

(Figure 6C). The overlap of ZD2-Cy5 binding with immunostaining of both EDB-FN and CD31 confirmed specific targeting of ZD2-Cy5 to PCa.

**Binding Study in Human Prostate Specimens of Varying Aggressiveness.** Tumor targeting of the ZD2

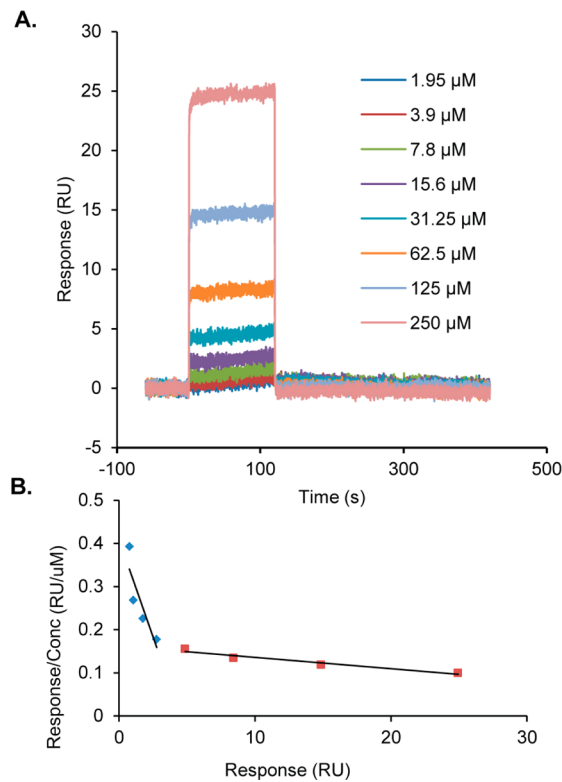


**Figure 3.** Characterization of the interaction between cyclic ZD2 and the EDB fragment using SPR. (A) Sensorgrams acquired by injecting different concentrations of ZD2 (denoted by different colors) onto the immobilized EDB protein are shown. (B) Scatchard plot of the binding levels. The slope of the trend lines represents  $-1/K_d$  for two different binding sites.

peptide was further assessed in human prostate tumor sections with varying Gleason scores, while a human prostate BPH tissue section was used as control. As shown in Figure 7, ZD2-Cy5 significantly binds to prostate tumors (GS7 and GS9), but not to the BPH tissue sections. The fluorescence intensity of ZD2-Cy5 in the tumor sections was found to correlate with the Gleason score-based tumor aggressiveness, with stronger staining seen in both the stromal and glandular areas of specimens with a higher Gleason score. This finding is consistent with a previous study that shows an overexpression of EDB-FN in prostate carcinoma compared with BPH.<sup>16,25</sup> A similar trend was observed with BC-1 immunofluorescence staining. These results demonstrate that the specific binding of ZD2 to EDB-FN also leads to effective binding of ZD2 to high-risk human prostate tumors, with the potential to differentiate between the tumor aggressiveness.

## DISCUSSION

Specific targeting to cancer biomarkers is essential for the development of noninvasive imaging technology, so as to facilitate accurate detection and efficacious therapy of high-risk PCa. EDB-FN is one of the hallmarks of EMT and its expression is elevated in post-EMT PCa cells.<sup>16</sup> EDB-FN is also involved in tumor angiogenesis.<sup>22</sup> Consequently, we identified the cyclic nonapeptide ZD2 specific to EDB-FN using phage display. The binding specificity of this peptide was first verified using the fluorescent probe ZD2-Cy5 ex vivo in post-EMT PC3 prostate cancer cells. EMT induction of PC3 cells by TGF- $\beta$  resulted in substantial up-regulation of EDB-FN. ZD2-Cy5 showed enhanced binding in post-EMT PC3 cells, but no binding in noninduced cells. The strong binding signal of ZD2-Cy5 was localized to the periphery of the induced PC3 cells, which is consistent with the fact that FN is an ECM protein. The tumor-specificity of the peptide was also demonstrated in

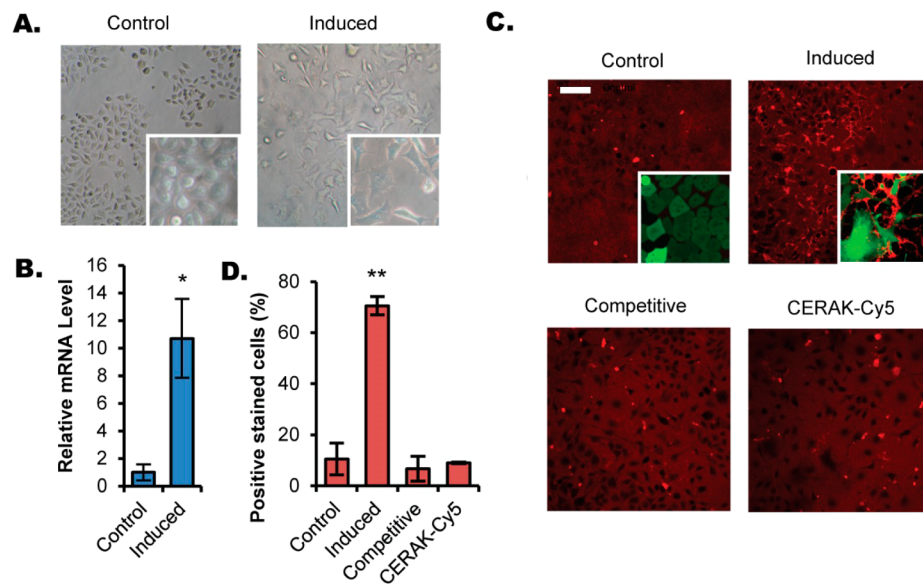


**Figure 4.** ZD2-Cy5 binding in PC3 cells. (A) Morphology of PC3 cells with and without TGF- $\beta$  induction. Images were taken by phase-contrast microscopy at 10 $\times$  and 40 $\times$  magnification (inset). (B) qRT-PCR analysis of EDB expression in PC3 cells with or without TGF- $\beta$  induction. (C) Representative confocal fluorescence images of ZD2-Cy5 binding in noninduced PC3 cells (control), induced PC3 cells (induced), and induced cells preincubated with 25  $\mu\text{M}$  free ZD2 peptide (competitive). Binding of CERAK-Cy5 in induced PC3 cells was used as a negative control. Scale bar: 100  $\mu\text{m}$ . Inset: magnified image shows binding of ZD2-Cy5 in noninduced and induced PC3 cells. GFP signal (green) delineates cell shape and ZD2-Cy5 signal (red) is clearly visible at cell periphery. (D) Percentage count of positively stained cells (cells with peptide-Cy5 binding on cell periphery) in different conditions.

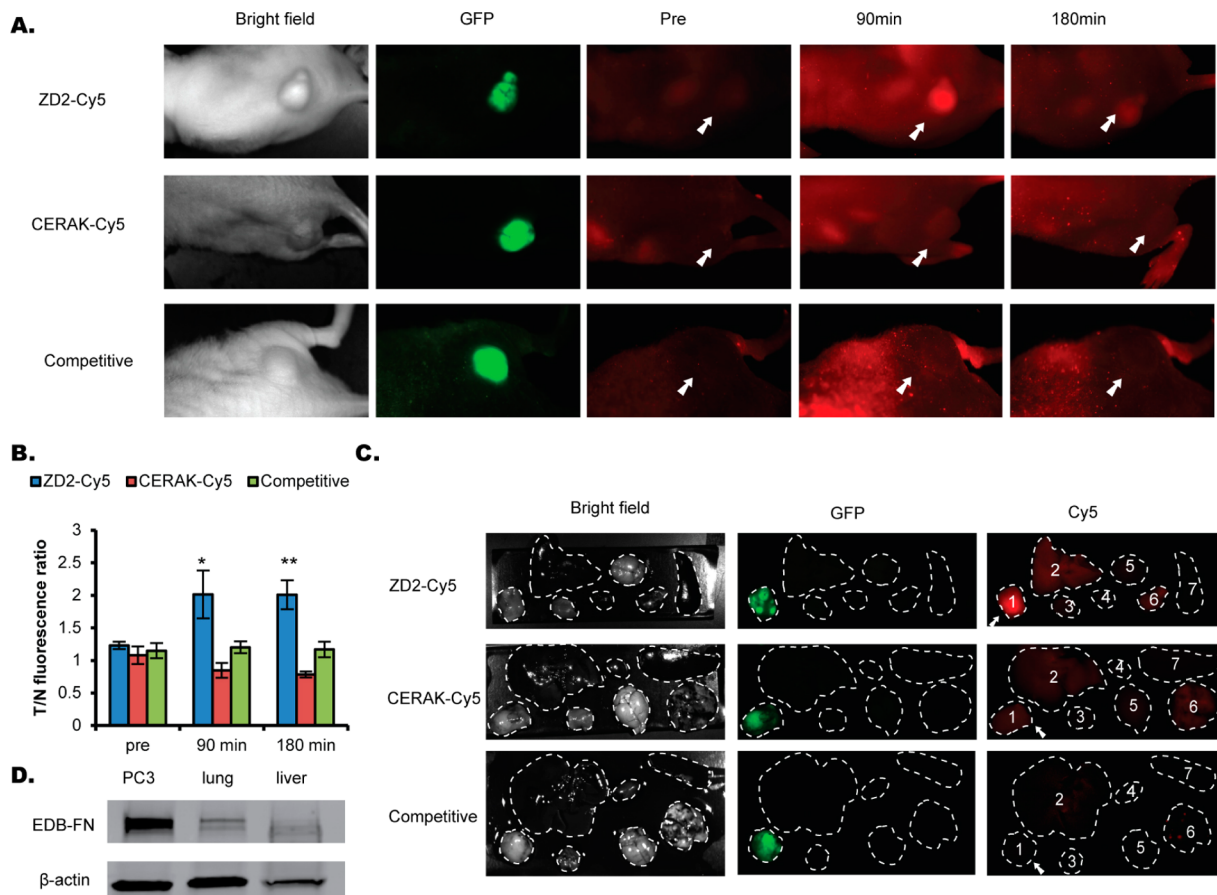


**Figure 5.** In vivo binding of ZD2-Cy5 in mice bearing PC3-GFP prostate cancer flank xenografts. (A) Representative fluorescence images of PC3-bearing mouse at 1 min before injection (labeled as pre) and 90 and 180 min after intravenous injection of 10 nmol ZD2-Cy5, nonspecific control CERAK-Cy5, and a mixture of 1  $\mu$ M cyclic ZD2 and 10 nmol ZD2-Cy5 (competitive). (B) Fluorescence intensity ratio between tumor and normal tissues (T/N ratio) from mice injected with ZD2-Cy5, CERAK-Cy5, or a mixture of 1  $\mu$ M cyclic ZD2 and 10 nmol ZD2-Cy5 (competitive). Images of tissues obtained 1 min before injection (pre), and 90 and 180 min after injection were analyzed ( $N = 3$ ). (C) Representative fluorescence images of organs harvested from PC3-GFP tumor-bearing mouse 5 h after injection of ZD2-Cy5, CERAK-Cy5, or a mixture of 1  $\mu$ M cyclic ZD2 and 10 nmol ZD2-Cy5 (competitive). The organs are represented with numbers: 1, tumor; 2, liver; 3, muscle; 4, heart; 5, brain; 6, lung; and 7, spleen. (D) Western blot analysis of the liver, lung, and tumor protein lysates. Antibody BC-1 was used to characterize the EDB-FN expression, and expression of  $\beta$ -actin was used as the loading control.

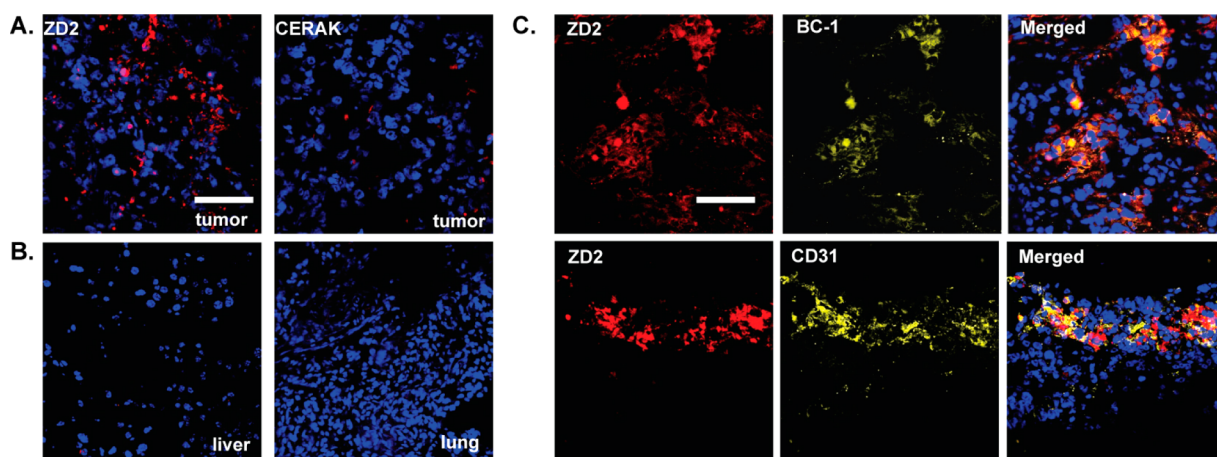


**Figure 6.** Histological analysis of tissue sections of PC3 tumors from mice injected with ZD2-Cy5 or CERAK-Cy5. (A) Representative fluorescence images of tumor sections from PC3 tumor xenografts injected with ZD2-Cy5 or CERAK-Cy5. (B) Representative fluorescence images of the liver and lung sections from the same mice showing nonbinding of ZD2-Cy5. Scale bar: 20  $\mu$ m. (C) Correlation of ZD2 distribution with EDB-FN (BC-1) distribution and blood microvessel distribution (anti-CD31) in the PC3 tumor sections. Scale bar: 20  $\mu$ m. Pseudocolors are assigned as follows: red, peptide; yellow, antibody; and blue, nucleus.

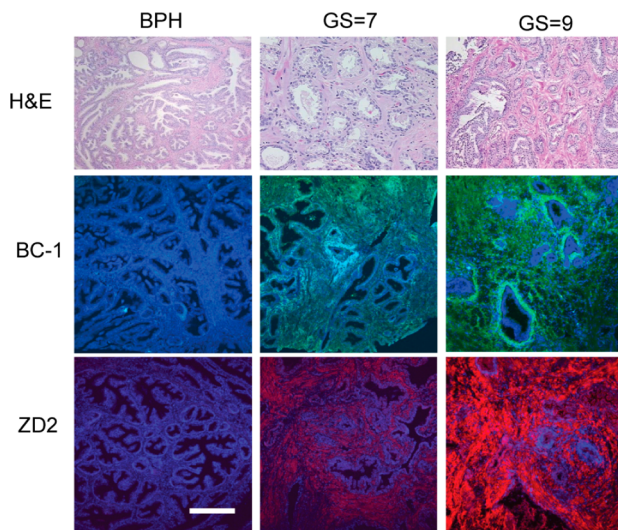


**Figure 7.** ZD2-Cy5 binding in human prostate sections with varying Gleason scores (GS7, 3 + 4, GS9, and 4 + 5) with BPH as a negative control. H&E staining, immunofluorescence staining with BC-1, and ZD2-Cy5 staining are shown. Scale bar: 100  $\mu$ m. Pseudocolors in the confocal images are assigned as follows: red, peptide; green, BC-1; and blue, nucleus.

mice bearing PC3-GFP prostate cancer xenografts and in human prostate tumor specimens with varying Gleason scores. Gleason score is the most commonly used pathological grading system for the clinical management of PCa. Our results suggest that EDB-FN is a potential marker of high-risk PCa and the ZD2 peptide is a viable probe for targeting this biomarker.

Currently, needle biopsy Gleason scoring is routinely used in the risk-stratified management and therapeutic intervention of PCa. The goal of this management strategy is to minimize treatment-related risks in patients who do not benefit from the treatment.<sup>26</sup> However, the accuracy of the diagnostic procedure is often compromised by the heterogeneity of PCa cells within the same prostate tissue and the inadequacy of prostate sampling from needle biopsy. Consequently, a molecular imaging technology that can noninvasively map all areas of the prostate tissue in high-risk PCa is more advantageous over invasive biopsy and could provide more accurate differential diagnosis. Since EDB-FN is a molecular marker of PCa, angiogenesis, and EMT, and is characteristic of high-risk PCa, the ZD2 peptide may open avenues in developing imaging agents for noninvasive molecular imaging and accurate diagnosis of PCa.<sup>27–29</sup> Although antibodies have been developed to target EDB-FN, small peptides are advantageous due to their lack of immunogenicity and cost-effective scale-up for mass production.

We have shown that ZD2-Cy5 can be used to effectively visualize PCa by fluorescence imaging. This fluorescent peptide probe or a further optimized probe could potentially serve to delineate the margins of high-risk PCa during image-guided surgery. This would facilitate the complete resection of high-risk prostate tumors while minimizing unnecessary removal of healthy tissue.<sup>30</sup> It is also possible to use this peptide for the development of targeted imaging agents for clinical imaging modalities, including SPECT, PET, and MRI, for noninvasive detection and differential diagnosis of high-risk PCa in the clinic. Currently, we are exploring the potential of the ZD2 peptide in the synthesis of targeted MRI contrast agents and PET probes for noninvasive molecular imaging of PCa.

The ZD2 peptide could also be used in developing targeted drug delivery systems to deliver therapeutics, including chemotherapeutics and therapeutic nucleic acids, and to improve their efficacy. Because of the increased expression of EDB-FN in the tumor ECM, the ZD2 peptide could facilitate rapid enrichment of the therapeutics in the tumor to improve tumor targeting efficiency, in turn minimizing systemic circulation of the therapeutics, reducing potential side effects, and enhancing uptake in cancer cells to improve therapeutic efficacy.

## CONCLUSIONS

Using phage display, we have identified a peptide CTVRTSADC (ZD2), which is specific to EDB-FN, for targeting PCa. ZD2 can specifically bind to EDB-FN produced by post-EMT PC3 prostate cancer cells, mouse prostate tumor xenografts, and to human prostate tissue specimens with high Gleason scores. The fluorescent ZD2 peptide probe can facilitate molecular imaging of PCa and image-guided surgery. The ZD2 peptide is a promising tool for the design of targeting agents for molecular imaging and targeted drug delivery in PCa diagnosis and therapy.

## MATERIALS AND METHODS

**Materials.** All reagents were used without further purification unless otherwise stated. Fmoc-protected amino acids and 2-chlorotriptyl chloride resin were purchased from Chem-Impex International, Inc. (Wood Dale, IL). Fmoc-12-amino-4,7,10-trioxadodecanoic acid was purchased from EMD Chemicals Inc. (Gibbstown, NJ). Sulfo-Cy5.0 NHS ester was purchased from Lumiprobe (Hallandale Beach, FL). Anhydrous *N,N*-diisopropylethyl amine (DIPEA) and *N,N*-dimethylformamide (DMF) were purchased from Alfa Aesar (Ward Hill, MA). Trifluoroacetic acid (TFA) was purchased from Oakwood Products, Inc. (West Columbia, SC). FastDigest enzymes for plasmid construction were purchased from Fermentas (Thermo Scientific Co., Rockford, IL). Anti-fibronectin monoclonal antibody (BC-1; ab154210) and FITC-conjugated goat polyclonal anti-mouse Fc (ab97264) were purchased from Abcam (Cambridge, UK). Rhodamine-Red-X conjugated goat polyclonal anti-rabbit IgG (H+L) was obtained from Jackson ImmunoResearch Lab (West Grove, PA).

**EDB Expression in *E. coli*.** The coding sequence for EDB was optimized by *GeneOptimizer* software algorithm and further synthesized (GeneArt, Regensburg, Germany) before being cloned into pQE-T7-1 expression vector (Qiagen, Valencia, CA). *Nde*I and *Pst*I restriction sites in the multicloning sites were used for insertion of EDB DNA segment, which resulted in the fusion of 10 His tags at the N-terminus of the EDB protein. The expression of EDB is regulated by a T7 promoter along with the control of a lac operator, as shown in Figure 1A. Successful ligation was verified by sequencing the inserted DNA on the recombinant plasmid. Primers used for EDB sequencing are 5'-GCAGCAGCCAACTCAGCT-3' (forward), and 5'-CCTCTAGAAATAATTTGTTAACCTT-3' (reverse). Sequencing was performed by CWRU Genomics Core. The recombinant plasmid was transformed into *E. coli* strain BL21(DE3)-T1 (Sigma-Aldrich, St Louis, MO) for EDB production. EDB expression was induced by 1 mM IPTG at the mid log phase of BL21, followed by incubation for 3 h. The bacteria were collected by centrifugation at 4000  $\times g$  for 5 min and lysed with lysozyme (Sigma-Aldrich, St Louis, MO) as

instructed by the manufacturer. Purification of EDB using 10 His tags was carried out with Ni Sepharose 6 Fast Flow (GE Healthcare, Waukesha, WI), followed by dialysis against water and lyophilization. The size and purity of the extracted EDB protein were determined by SDS-PAGE.

**Phage Screening.** The Ph.D C7C library (New England Biolabs, Beverly, MA) was used to screen for EDB-specific cyclic nonapeptides. Candidate peptides were selected by panning for four rounds. In each round, purified EDB fragment (100  $\mu$ g/mL) was immobilized by overnight coating on nontreated 96-well plates (Corning Costar, Tewksbury, MA, USA) 4 °C. BSA (0.5%) was used to block nonspecific binding (1 h, room temperature) followed by incubating with phages for 1 h at room temperature. Extensive washing with PBST (0.1%, 0.3%, 0.5% Tween-20, respectively, three times) was performed to remove nonbinding phages before eluting the bound phages with 0.1 M glycine-HCl (pH 2.2) and neutralizing with Tris-HCl (pH 9.1). The eluted phages were titered and amplified with *E. coli* (ER2758), according to the user's manual. Amplified phages in the medium were purified by ultrafiltration and PEG/NaCl precipitation. At the end of round 4, properly diluted phages were cultured on LB/IPTG/Xgal plates, and DNA from 29 random blue plaques was sequenced using supplied primers (New England Biolabs) along with the phage library. Peptide sequences were acquired after translating the corresponding DNA sequences.

**Use of SPR for Characterizing the Interaction between Cyclic ZD2 and EDB.** ZD2 peptide, bearing the sequence CTVRTSADC, was synthesized using standard solid-phase synthesis from Fmoc-protected amino acids on a 2-chlorotriptyl chloride resin. Cyclization of the peptide was carried out by exposing the peptide to air in 10% DMSO at pH 7.0. Purification of the cyclic peptide was done using RP-HPLC followed by lyophilization. Elution buffer (PBS containing 500 mM imidazole) containing about 4 mg/mL EDB protein was desalted with Zebra Spin Desalting Columns (Thermo Scientific, Rockford, IL) prior to immobilization. SPR was performed using Biacore T100 (GE healthcare, Waukesha, WI). For the affinity experiments, all the samples were in phosphate buffered saline (pH 7.4) containing 150 mM NaCl and 0.05% P20. The same buffer was also used as the running buffer. To immobilize the EDB protein, the active and reference flow cells of a CMS series S sensor chip (GE Healthcare Life Science, Ohio, USA) were activated with 1-ethyl-3-(3-(dimethylamino)-propyl)carbodiimide hydrochloride (EDC) and *N*-hydroxysuccinimide (NHS) for 7 min, according to the manufacturer's instructions. EDB protein diluted to 25  $\mu$ g/mL with acetate buffer (pH 4.5) was injected over the active cell for 3 min at 10  $\mu$ L/min, resulting in an immobilization level of 2000 RU. Both the reference flow cell and active flow cell were blocked with ethanolamine, pH 8.5 for 7 min. The system was then switched to running buffer and different concentrations of the peptide were injected for 120 s at 50  $\mu$ L/min, with 5 min of dissociation. The binding data was analyzed using the Scatchard plot. Affinity was calculated by fitting data points into a linear trend line using Microsoft Office Excel software. Slope of the trend line represents  $-1/K_d$ .

**Fluorescence Imaging Probe Synthesis.** ZD2 peptide was synthesized in solid phase as previously described. A short PEG (Fmoc-12-amino-4,7,10-trioxadodecanoic acid) was conjugated to the deprotected amine group as a linker. Sulfo-Cy5.0 NHS ester was sequentially conjugated to form fluorescent ZD2 probe. The probe was treated with TFA

solution (TFA 94%, 1,2-ethanedithiol 2.5%, triisobutylsilane 2.5%, water 1.0%) and precipitated with cold ether. Cyclization of the peptide was carried out by exposing the peptide to air in 10% DMSO at pH 7.0. Purification of the cyclic peptide was done using RP-HPLC followed by lyophilization. The final product, denoted as ZD2-Cy5, was characterized by MALDI-TOF mass spectrometry.

**In Vitro Target Binding.** PC3 cells were purchased from American Type Culture Collection (ATCC, Manassas, VA), and maintained in RPMI/10% FBS medium. The cells were transfected with lentivirus to express green fluorescent protein (GFP), as previously reported.<sup>31</sup> Glass-bottom dishes were precoated with a thin layer of matrigel for cell culture to facilitate the retention of cell-secreted protein on the glass surface. To induce EMT, the PC3 cells were cultured in the presence of TGF- $\beta$  (5 ng/mL) for 5 days. Induced cells were maintained in medium containing 250 nM ZD2-Cy5 for 1 h and peptide binding was monitored with confocal microscopy. Intense shaking and washing were avoided for successful retention of secreted EDB-FN on the plate. Noninduced PC3 cells were also incubated with ZD2-Cy5. Competitive study was performed by preincubating the cells with 25  $\mu$ M nonlabeled ZD2 peptide, followed by the addition of 250 nM ZD2-Cy5. Binding of 250 nM CERAK-Cy5 on the induced PC3 cells was used as a control. Regions of interest (ROIs) in three independent experiments were selected to compare the percent count of positively stained cells (cells with peptide-Cy5 binding in cell periphery) in different conditions.

**qRT-PCR.** Total RNA was extracted from the cell samples using an RNeasy Plus Kit (Qiagen). RNA was reverse-transcribed into cDNA using the High Capacity cDNA Transcription Kit (Applied Biosystems, Foster City, CA). Semiquantitative real-time PCR was carried out using a SYBR Green Master Mix (Life Technologies), according to the manufacturer's recommendations. RNA expression for the individual genes examined was normalized to the corresponding GAPDH RNA signals. Both cDNA synthesis and real-time PCR were performed in the Mastercycler realplex2 (VWR International, West Chester, PA). Relative mRNA expression levels were calculated using the  $2^{-\Delta\Delta CT}$  method.<sup>32</sup> The following primer sequences were used: 5'-GCAGCCCCACAGT-GGAGTAT-3' (EDB forward), 5'-GGAGCAAGGTTGATT-TCTT-3' (EDB reverse); 5'-ACCCAGAAGACTGTGG-ATGG-3' (GADPH forward), and 5'-TCTAGACGGCAGG-TCAGGTC-3' (GADPH reverse).

**In Vivo Fluorescence Imaging.** NIH athymic nude male mice (4–5 weeks) were maintained at the Athymic Animal Core Facility at Case Western Reserve University, according to the animal protocols approved by the Institutional Animal Care and Use Committee. Mice were subcutaneously injected with 50  $\mu$ L cell suspension in matrigel ( $4 \times 10^7$  cells/mL) in the flanks. Two to three weeks after inoculation, the tumors reached an average size of 0.7 cm in diameter. The mice were intravenously injected with ZD2-Cy5 or CERAK-Cy5 (10 nmol). For the in vivo competitive binding study, 1  $\mu$ mol of cyclic ZD2 without Cy5 was coinjected with 10 nmol ZD2-Cy5. The targeted binding of ZD2-Cy5 to the prostate tumor was assessed in vivo by Maestro FLEX In Vivo Imaging System (PerkinElmer, Waltham, MA) using a yellow filter set (spectral range of 630–800 nm, 1000 ms exposure time) for Cy5 and a blue filter set (spectral range 500–720 nm, 400 ms exposure time) for GFP. During imaging, the imaging bed was kept at 37 °C. Mice were anesthetized by isofluorane inhalation via a nose

cone attached to the imaging bed. The mice were imaged over 3 h post-injection. After 5 h, the mice were sacrificed and the tumor and organs were imaged with Maestro FLEX In Vivo Imaging System. For analyzing probe binding in the tumor, regions of interest (ROIs) in live mouse images were selected from the flank tumor and leg muscle.

**Immunostaining of Mouse Tissues.** Tumors and organs collected from mice after fluorescence imaging were embedded in optimum cutter temperature compound (OCT) before being frozen at  $-80^{\circ}\text{C}$ . OCT blocks were cut at  $5\ \mu\text{m}$  in the dark. Cold acetone was used for fixing the sections. For assessing peptide distribution in different organs, sections from the organ were directly counter-stained with DAPI and a coverslip was placed. For immunostaining with anti-EDB antibody and anti-CD31 antibody, the sections were blocked with 0.5% BSA for 1 h at room temperature before applying antibody solutions. All the sections were examined by confocal laser scanning microscopy.

**SDS-PAGE and Western Blotting Analysis.** Tissues from the mice were lysed with T-PER Tissue Protein Extraction Reagent (Thermo Scientific, Rockford, IL) supplemented with PMSF (Sigma, St. Louis, MO, USA) and protease inhibitors (Sigma, St. Louis, MO, USA), according to manufacturer's instructions. Protein concentration in the extracted lysates was measured with bicinchoninic acid (BCA) assay kit (Thermo Scientific, Rockford, IL). Proteins ( $20\ \mu\text{g}$ ) were loaded onto 4–15% Mini-protein TGX precast gel (Biorad, Hercules, CA) in Tris/glycine/SDS buffer for electrophoresis. Bacterial lysates ( $20\ \mu\text{L}$ ) were directly loaded without the BCA assay. After SDS-PAGE, the protein bands were visualized by Coomassie blue staining after migration. For Western blotting, the proteins in the SDS-PAGE gel were transferred onto PVDF membranes (Invitrogen, Carlsbad, CA). Membranes were blotted with 0.5% BSA for 1 h at room temperature and incubated with anti-EDB antibody (BC-1, 1:2000) for 1 h. The membranes were then washed and incubated with FITC-conjugated antimouse secondary antibody (1:1000) in 0.5% BSA. After extensive washing, a Typhoon Phosphor imager (General Electric, Fairfield, CT) was used for processing the membrane.

**Peptide and Antibody Binding in Human Prostate Specimens.** Human prostate sections were acquired from OriGene (Rockville, MD). Frozen tissue sections ( $5\ \mu\text{m}$ ) imbedded in OCT were used for immunostaining and peptide staining. Paraffin embedded samples were deparaffinized and processed with standard antigen retrieval methods. The sections were permeabilized and fixed with cold acetone followed by 0.5% BSA blocking for 1 h at room temperature. ZD2-Cy5 ( $5\ \mu\text{M}$ ) was then incubated with the tissue sections. Slides were counter-stained with DAPI and a coverslip was placed using Prolong Gold reagent (Invitrogen, Carlsbad, CA) before imaging. Immunostaining was performed using similar protocol as described for the mouse tissues. The stained tissues were imaged on an Olympus FV1000 confocal laser scanning microscope.

**Statistical Analysis.** All the data are presented as mean  $\pm$  SD unless otherwise stated. When two groups were compared, the two-tailed Student's *t*-test was used ( $p < 0.05$  was considered significant).

## AUTHOR INFORMATION

### Corresponding Author

\*E-mail: zx125@case.edu. Phone: 216-368-0187. Fax: 216-368-4969.

### Notes

The authors declare the following competing financial interest(s): Drs. Lu and Zhu are co-founders of Prostate Theranostics, LLC..

## ACKNOWLEDGMENTS

This project was supported in part by the NIH grant R01 EB00489 and a pilot grant from the Wallace H. Coulter Foundation. We thank Dr. Amita Vaidya for proof-reading.

## REFERENCES

- (1) Siegel, R., Naishadham, D., and Jemal, A. (2012) Cancer statistics, 2012. *Ca-Cancer J. Clin.* 62, 10–29.
- (2) Barry, M. J. (2001) Clinical practice. Prostate-specific-antigen testing for early diagnosis of prostate cancer. *N. Engl. J. Med.* 344, 1373–7.
- (3) Dhanasekaran, S. M., Barrette, T. R., Ghosh, D., Shah, R., Varambally, S., Kurachi, K., Pienta, K. J., Rubin, M. A., and Chinnaiyan, A. M. (2001) Delineation of prognostic biomarkers in prostate cancer. *Nature* 412, 822–6.
- (4) Melnikow, J., LeFevre, M., Wilt, T. J., and Moyer, V. A. Counterpoint: Randomized trials provide the strongest evidence for clinical guidelines: The US Preventive Services Task Force and Prostate Cancer Screening. *Med. Care* 51, 301–3.
- (5) Moyer, V. A. Screening for prostate cancer: U.S. Preventive Services Task Force recommendation statement. *Ann. Int. Med.* 157, 120–34.
- (6) Wernert, N. (1997) The multiple roles of tumour stroma. *Virchows Arch.* 430, 433–43.
- (7) Park, J., and Schwarzbauer, J. E. (2014) Mammary epithelial cell interactions with fibronectin stimulate epithelial-mesenchymal transition. *Oncogene* 33, 1649–57.
- (8) Alisson-Silva, F., Freire-de-Lima, L., Donadio, J. L., Lucena, M. C., Penha, L., Sa-Diniz, J. N., Dias, W. B., and Todeschini, A. R. (2013) Increase of O-glycosylated oncofetal fibronectin in high glucose-induced epithelial-mesenchymal transition of cultured human epithelial cells. *PLoS One* 8, e60471.
- (9) Borsi, L., Carnemolla, B., Neri, D., and Zardi, L. (2001) Use of human recombinant antibodies to the marker of angiogenesis ED-B in cancer therapy. *Tumori* 87, S8–S10.
- (10) Hajitou, A., Pasqualini, R., and Arap, W. (2006) Vascular targeting: recent advances and therapeutic perspectives. *Trends Cardiovasc. Med.* 16, 80–8.
- (11) Mani, S. A., Guo, W., Liao, M. J., Eaton, E. N., Ayyanan, A., Zhou, A. Y., Brooks, M., Reinhard, F., Zhang, C. C., Shipitsin, M., et al. (2008) The epithelial-mesenchymal transition generates cells with properties of stem cells. *Cell* 133, 704–15.
- (12) Balanis, N., Wendt, M. K., Schiemann, B. J., Wang, Z., Schiemann, W. P., and Carlin, C. R. (2013) Epithelial to mesenchymal transition promotes breast cancer progression via a fibronectin-independent STAT3 signaling pathway. *J. Biol. Chem.* 288, 17954–67.
- (13) Kaspar, M., Zardi, L., and Neri, D. (2006) Fibronectin as target for tumor therapy. *Int. J. Cancer* 118, 1331–9.
- (14) Ratliff, T. L., Kavoussi, L. R., and Catalona, W. J. (1988) Role of fibronectin in intravesical BCG therapy for superficial bladder cancer. *J. Urol.* 139, 410–4.
- (15) Tuxhorn, J. A., Ayala, G. E., and Rowley, D. R. (2001) Reactive stroma in prostate cancer progression. *J. Urol.* 166, 2472–83.
- (16) Albrecht, M., Renneberg, H., Wennemuth, G., Moschler, O., Janssen, M., Aumuller, G., and Konrad, L. (1999) Fibronectin in human prostatic cells in vivo and in vitro: expression, distribution, and pathological significance. *Histochem. Cell Biol.* 112, 51–61.
- (17) Freire-de-Lima, L., Gelfenbeyn, K., Ding, Y., Mandel, U., Clausen, H., Handa, K., and Hakomori, S. I. (2011) Involvement of O-glycosylation defining oncofetal fibronectin in epithelial-mesenchymal transition process. *Proc. Natl. Acad. Sci. U. S. A.* 108, 17690–5.

- (18) Suer, S., Sonmez, H., Karaaslan, I., Baloglu, H., and Kokoglu, E. (1996) Tissue sialic acid and fibronectin levels in human prostatic cancer. *Cancer Lett.* 99, 135–7.
- (19) Sonmez, H., Suer, S., Karaaslan, I., Baloglu, H., and Kokoglu, E. (1995) Tissue fibronectin levels of human prostatic cancer, as a tumor marker. *Cancer Biochem. Biophys.* 15, 107–110.
- (20) Inufusa, H., Nakamura, M., Adachi, T., Nakatani, Y., Shindo, K., Yasutomi, M., and Matsuura, H. (1995) Localization of oncofetal and normal fibronectin in colorectal cancer. Correlation with histologic grade, liver metastasis, and prognosis. *Cancer* 75, 2802–8.
- (21) Menzin, A. W., Loret de Mola, J. R., Bilker, W. B., Wheeler, J. E., Rubin, S. C., and Feinberg, R. F. (1998) Identification of oncofetal fibronectin in patients with advanced epithelial ovarian cancer: detection in ascitic fluid and localization to primary sites and metastatic implants. *Cancer* 82, 152–8.
- (22) Barron, D. A., and Rowley, D. R. (2012) The reactive stroma microenvironment and prostate cancer progression. *Endocr. Relat. Cancer* 19, R187–204.
- (23) Jaggi, M., Nazemi, T., Abrahams, N. A., Baker, J. J., Galich, A., Smith, L. M., and Balaji, K. C. (2006) N-cadherin switching occurs in high Gleason grade prostate cancer. *Prostate* 66, 193–9.
- (24) Wilkinson, K. D. (2004) Quantitative analysis of protein-protein interactions, in *Protein-Protein Interactions*, pp 15–31, Springer.
- (25) Jankovic, M. M., and Kosanovic, M. M. (2008) Fibronectin pattern in benign hyperplasia and cancer of the prostate. *Dis. Markers* 25, 49–58.
- (26) Glass, A. S., Cary, K. C., and Cooperberg, M. R. (2013) Risk-based prostate cancer screening: who and how? *Curr. Urol. Rep.* 14, 192–198.
- (27) Locher, R., Erba, P. A., Hirsch, B., Bombardieri, E., Giovannoni, L., Neri, D., Durkop, H., and Menssen, H. D. (2014) Abundant in vitro expression of the oncofetal ED-B-containing fibronectin translates into selective pharmacodelivery of (131)I-L19SIP in a prostate cancer patient. *J. Cancer Res. Clin. Oncol.* 140, 35–43.
- (28) Wu, X., Yu, G., Lindner, D., Brady-Kalnay, S. M., Zhang, Q., and Lu, Z. R. (2014) Peptide-targeted high-resolution molecular imaging of prostate cancer with MRI. *Am. J. Nucl. Med. Mol. Imaging* 4, 525–36.
- (29) Wu, X., Burden-Gulley, S. M., Yu, G. P., Tan, M., Lindner, D., Brady-Kalnay, S. M., and Lu, Z. R. Synthesis and evaluation of a peptide-targeted small molecular Gd-DOTA monoamide conjugate for MR molecular imaging of prostate cancer. *Bioconjugate Chem.* 23, 1548–56.
- (30) Vahrmeijer, A. L., Hutteman, M., van der Vorst, J. R., van de Velde, C. J., and Frangioni, J. V. (2013) Image-guided cancer surgery using near-infrared fluorescence. *Nat. Rev. Clin. Oncol.* 10, 507–18.
- (31) Tan, M., Burden-Gulley, S. M., Li, W., Wu, X., Lindner, D., Brady-Kalnay, S. M., Gulani, V., and Lu, Z.-R. (2012) MR molecular imaging of prostate cancer with a peptide-targeted contrast agent in a mouse orthotopic prostate cancer model. *Pharm. Res.* 29, 953–960.
- (32) Schmittgen, T. D., and Livak, K. J. (2008) Analyzing real-time PCR data by the comparative CT method. *Nat. Protoc.* 3, 1101–1108.